Modeling of the reflectance function for multilayered structures with imperfect adherence conditions at interfaces

A. Loukkal, M. Lematre, M. Bavencoffe et M. Lethiecq
GREMAN UMR 7347, Univ. de Tours/CNRS/INSA-CVL, site INSA, 3 rue de la Chocolaterie, 41000 Blois, France
abderrahmane.loukkal@univ-tours.fr

The microelectronics industry is expressing an increased demand for the development of non-destructive tools and methods for health control and diagnostics in multilayered structures, including problems such as delaminations, inclusions and microcracks. In order to obtain a quantitative characterization of elastic properties and interfacial adhesion properties in multilayered structures, we aim to apply the V(z) method used in acoustic microscopy in a near future. This technique allows to measure the velocities of guided waves or to rebuild the reflectance function. Both of them are sensitive to material properties and interface quality. Thus, as far as the reflectance function is concerned, in this study we propose models for calculating the reflectance functions on multilayered structures by taking into account imperfect interfaces between the layers. A study was conducted to evaluate numerically the influence of the properties of the imperfect interface on the reflectance function. The imperfect interfaces were numerically modeled by interfacial layers with thicknesses much smaller than those of the other layers and the characteristic wavelength in this layer.

1 Introduction

There are two main boundary conditions for solid / solid interfaces. The first condition is that of the perfect rigid contact where the sets of stresses and displacements are transmitted from one layer to another [1][2]. The second is that of the slip boundary condition through which the normal stress and displacement components are transmitted, the shear stress vanishes and the horizontal component of the displacement is discontinuous [3].

On the basis of the transfer matrix method [2,4–6], two different models have been implemented in MATLAB®, dealing respectively with isotropic and anisotropic materials.

These models have been presented in [7,8] for imperfect adherence conditions between two semi infinite half spaces. In the present work, we propose to use these models to study the adherence quality between layers in multilayered structures.

2 Case of isotropic materials

2.1 Theoretical background

We consider a multilayered isotropic structure consisting of N layers (Figure 1). Each layer k of this structure has a thickness d_k and the total thickness is equal to D. The multilayer is immersed in water (media 0 and N + 1) and a longitudinal wave is assumed to be incident on the multilayer with an angle θ_0.

The displacements and stresses existing at the top of a layer are connected to those of the base of the same layer by means of a layer transfer matrix. The continuity conditions then make it possible to establish a global transfer matrix resulting from the product of the transfer matrices of the successive layers. This global matrix allows the displacements and stresses of the top layer to be related to those of the bottom one. In the model, imperfect interfaces are modeled by an interfacial layer. The latter possesses a thickness much smaller than the wavelengths propagating in the medium.

The imperfect interface layer has been modeled by a viscoelastic material whose properties vary according to its structure [8]. This virtual material obeys to the Maxwell model. Such a material is represented as a series association of a hookean spring and a purely viscous damper. The viscoelasticity has been described by an imaginary component in the elastic coefficients of the material constituting the interface layer.

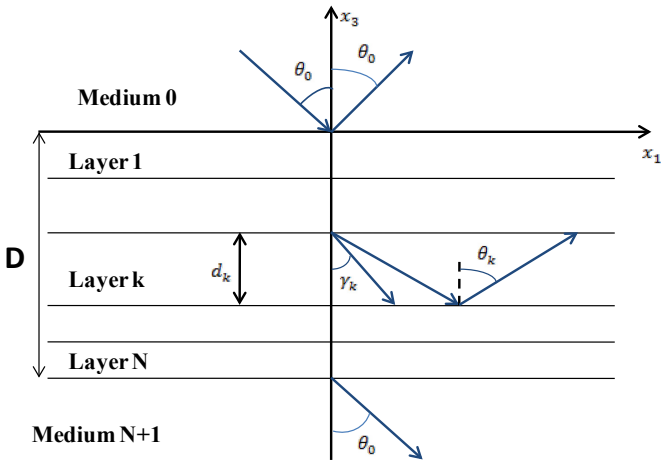

Figure 1: Multilayered structure geometry.

Thus, the bulk modulus and the shear modulus of the interfacial layer are respectively:

$$K = K_0 + (K_\infty - K_0)\left(\frac{\omega^2\tau^2}{1+\omega^2\tau^2} - i\frac{\omega\tau}{1+\omega^2\tau^2}\right) \quad (1)$$

$$\mu = \mu_\infty\left(\frac{\omega^2\tau^2}{1+\omega^2\tau^2} - i\frac{\omega\tau}{1+\omega^2\tau^2}\right) \quad (2)$$

where K_0 is the bulk modulus at the low frequency limit (corresponding to a liquid state); K_∞ and μ_∞ are respectively the bulk and the shear moduli of the material at the high frequency limit (corresponding to a solid state); ω is the angular frequency ($\omega = 2\pi f$, with f the frequency of the excitation signal); $\tau = \eta/\mu_\infty$ is the relaxation time and η is the static viscosity.

Parameters K_0, K_∞ and μ_∞ have been selected to match those of an epoxy resin [9]. Their values are displayed in Table 1.

Table 1: Elastic moduli of the viscoelastic interfacial medium.

K_0	K_∞	μ_∞
$1.9\ GPa$	$3.6\ GPa$	$1.2\ GPa$

The modification of the non-dimensional product parameter $\omega\tau$ makes it possible to change the mechanical properties of the interface layer. If we vary the value of this parameter from 0 to $+\infty$, the material constituting this layer can behave as an ideal fluid towards a solid in regard to the propagating waves. Indeed, Figure 2 shows that the imaginary part of the shear modulus of the viscoelastic material is maximal for $\omega\tau = 1$. Below the value 1, the imaginary part clearly dominates the real one, which results in an exacerbated dissipation property of the interface layer,

since the latter tends towards a liquid state. For values of $\omega\tau$ greater than 10 the shear modulus reaches a threshold equal to the value of the shear modulus of the material in its purely solid state. Thus, varying the value of this parameter makes it possible to simulate a degradation of the adherence quality which can be physically explained by the presence of defects such as delaminations [9].

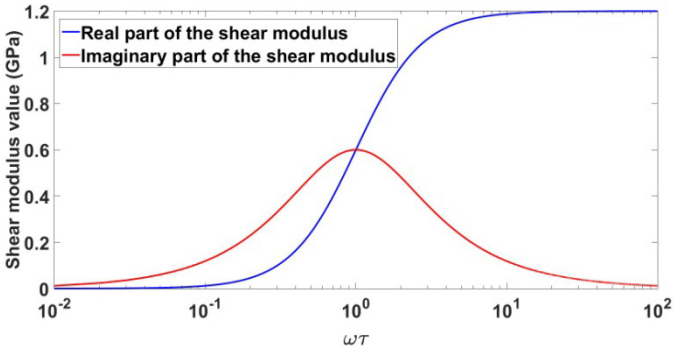

Figure 2: Evolution of the real and imaginary parts of the shear modulus with respect to the parameter $\omega\tau$.

2.2 Simulations and analysis

A numerical study was conducted in order to observe the influence of the product $\omega\tau$ on the evolution of the reflectance function for a bilayer consisting of 20 μm thick aluminum and steel layers with an imperfect interface (h thickness), as displayed with bold lines on Figure 3. The simulations were obtained for an incident wave frequency equal to 100 MHz and the results are presented on Figure 4. In this figure, the incident angles are limited to 40° since the magnitude of the reflectance function is equal to 1 beyond this value.

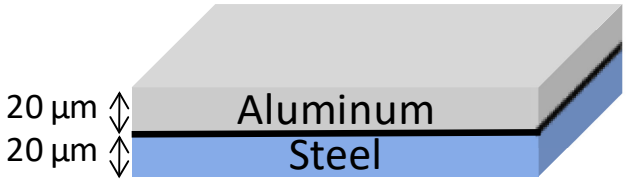

Figure 3: Isotropic multilayered structure with an imperfect interface.

The observation of Figure 4 reveals that the values of the reflectance functions for the incidence angle range from 0 to 40 degrees tend to decrease when the value of $\omega\tau$ decreases, corresponding to an increase of the fluid fraction. The reduction of the reflectance function is explained by the increased dissipative effect of the interface layer due to the decrease of the value of $\omega\tau$. These simulation results are in line with the behavior of the viscoelastic material shear modulus shown in Figure 2.

To summarize, the significant decrease in the reflection coefficient for the values of $\omega\tau \leq 1$ can be explained by the predominance of the dissipative phase of the interface material. Therefore, using a product $\omega\tau$ within the range $0 \leq \omega\tau \leq 1$ will be preferable to simulate a loss of adherence at the interface. Experimentally, the presence of the fluid fraction can be related to a delamination at the interface in the studied zone.

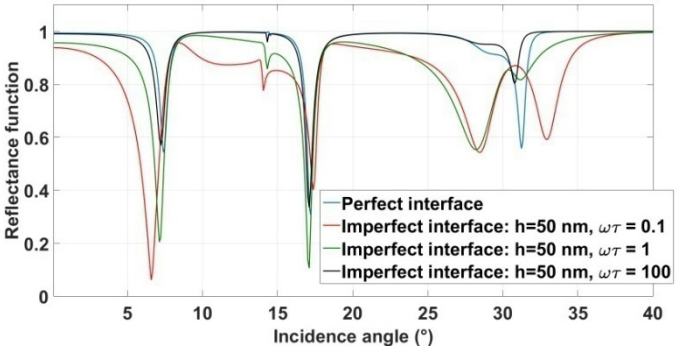

Figure 4: Magnitude of the reflectance functions obtained for multilayers containing perfect and imperfect interfaces with variable values of the product $\omega\tau$.

In order to verify the coherence of the numerical results, a comparison between reflectance functions obtained with perfect and imperfect interfaces with variable thicknesses and high values of $\omega\tau$ has been performed. The $\omega\tau$ value is set at 100 which corresponds pretty much to a welded contact at the interface considered in its solid state as illustrated by Figure 2.

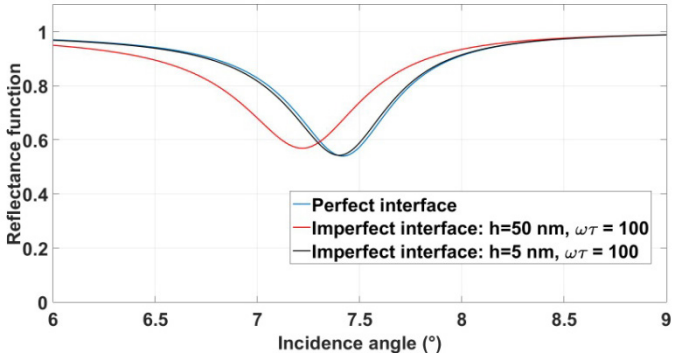

Figure 5: Comparison between the magnitude of the reflectance functions obtained for a multilayer with a perfect interface and multilayers containing imperfect interfaces with $\omega\tau = 100$ and variable thicknesses.

Figure 5 shows a comparison between the reflectance functions obtained in the case of a perfect interface and two imperfect interfaces at a frequency of 100 MHz for the multilayered structure described in Figure 3. The highly reduced incidence angle range ($6° \leq \theta_0 \leq 9°$) has been deliberately selected for this simulation for readability purposes, because the curves could not be discriminated for wider ranges. Indeed, for the standard incidence angle range, the correlation coefficient between the perfect interface and the imperfect ones ranges from 0.87 for $h = 50\ nm$ to 0.99 for $h = 5\ nm$. It is notable in this figure that the imperfect interfaces having a high value of $\omega\tau$ adopt a behavior very close to that of the perfect interface and all the more so as the interface layer thickness decreases.

3 Case of anisotropic materials

3.1 Theoretical background

The non-perfect interface model used for anisotropic materials does not rely on the viscoelasticity of the

interfacial layer. Here, the interface layer is represented by a virtual orthotropic material containing cylindrical pores parallel to the interface [7] that can form an angle φ with respect to the sagittal plane. We limited our present study to the case of cylindrical pores parallel to the sagittal plane ($\varphi = 0°$), which is chosen to be the x_1 axis, as shown in Figure 6. The degradation of the adherence quality between two layers is taken into account by an increase of the modeled porosity.

Dealing with this model, the first step consists in obtaining the elastic constants of the solid phase of the porous material considered. To do this, the Hill's approximation allows to calculate the elastic moduli necessary to describe an isotropic material obtained from the elastic parameters of the anisotropic material constituting the layer located below the imperfect interface [10]. In a second step, these isotropic elastic moduli are integrated in the Christensen's two-phase composite model to extract the effective anisotropic elastic constants of the interfacial material [11].

The Hill's approximation consists in homogenizing the elastic moduli of an anisotropic material, considering that they possess intermediate values between the elastic moduli obtained with the Reuss [12] and Voigt [13] approximations.

The bulk and shear moduli of the interfacial layer obtained via Hill's approximation are the following:

$$K = \frac{K_v + K_r}{2} \quad (3)$$

$$G = \frac{G_v + G_r}{2} \quad (4)$$

where G_v, K_v and G_r, K_r are respectively the shear and bulk moduli calculated using the Voigt and Reuss approximations.

These moduli are then incorporated in the Christensen's composite model and a porosity factor P is set ($0 \leq P \leq 1$) in order to extract the six independent elastic constants C_{11}, $C_{22} = C_{33}$, $C_{12} = C_{13}$, C_{23}, C_{44} and $C_{55} = C_{66}$.

Within the frame of the Christensen's model, in order to get the effective interfacial elastic constants, two shear moduli noted μ_{12} and μ_{23} must be calculated. Referring to Figure 6, they respectively correspond to the shear modulus in the pores direction (along the x_1 axis) and the transverse shear modulus (along the x_2 axis). The evolution of these moduli with respect to the porosity is displayed on Figure 7.

Figure 7 shows that both shear moduli decrease when the porosity factor increases. This was expected since the shear moduli are dependent on the presence of a solid medium. Therefore when the porosity equals 1 both shear moduli vanish.

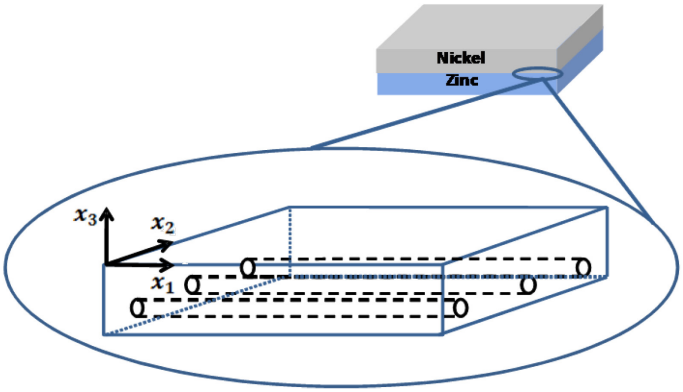

Figure 6: Representation of the anisotropic bilayer with the detailed structure of the imperfect interface layer.

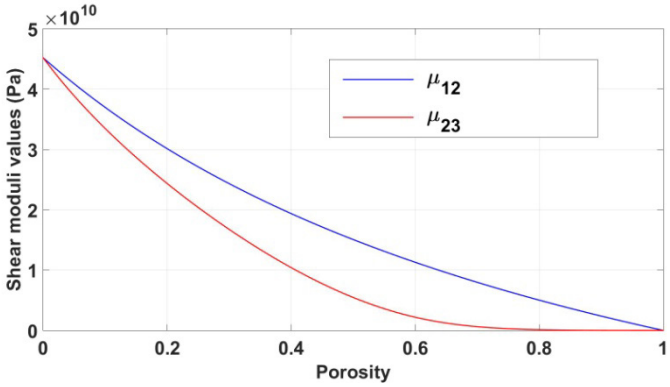

Figure 7: Evolution of the shear moduli μ_{12} and μ_{23} as a function of the porosity of the interfacial layer.

3.2 Simulations and analysis

The adhesion quality at the interface between two layers is dependent on the value of the porosity of the interface layer. Experimentally, an increase in the porosity coefficient is synonymous of an increased presence of delamination defects.

Figure 8 illustrates the evolution of the reflectance function as a function of the porosity coefficient for a bilayer composed of a 20 μm Nickel layer, a 500 nm interface layer and a 20 μm Zinc layer. . The mechanical properties [14][15] of these materials are displayed in Table 2.

Table 2: Mechanical properties of the materials constituting the anisotropic bilayer.

Material	Stiffness constants (GPa)	Density (kg/m^3)
Nickel	$C_{11} = 270$ $C_{12} = 170$ $C_{44} = 123$	8900
Zinc	$C_{11} = 165$ $C_{33} = 61.8$ $C_{44} = 39.6$ $C_{12} = 31.1$ $C_{13} = 50$	7130

The simulations have been conducted for an azimutal angle equal to zero in relation to the crystallographic axes of the materials, whose elastic constants are displayed in Table 2. The frequency of the incident wave on this multilayer is set to 100 MHz.

In Figure 8, the incident angles are limited to 40° since the magnitude of the reflectance function is equal to 1 beyond this value.

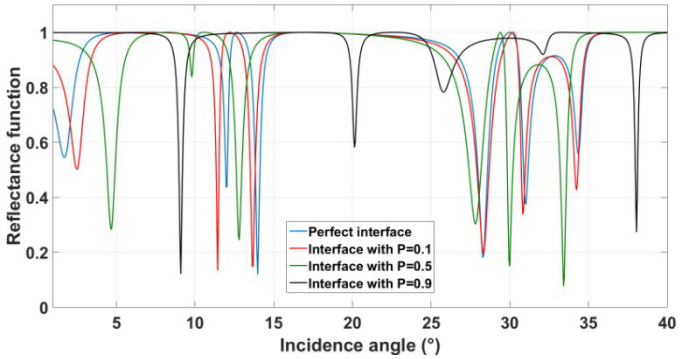

Figure 8: Magnitude of the reflectance functions obtained for multilayers containing 500 nm thick imperfect interfaces with variable porosities.

In the case of anisotropic materials, the model used shows very little difference between perfect and imperfect interfaces for very small thicknesses, with respect to the incident wave frequency, of the imperfect interface layer. This might be due to the obtainment of the solid phase of the virtual porous interfacial material by Hill's approximation from the Zinc inferior layer. Indeed, the propagating waves might be barely affected by the medium transition for very thin interface layers.

In order to fix that issue, we thus increased the thickness of the imperfect interface up to 500 nm until seeing significant differences, especially concerning the peaks positions. This value is still much smaller than that of the effective layers.

We define δ as the wavelength to thickness ratio calculated for a SH wave propagating in the interfacial material. The speed of a SH wave C_{SH} is calculated as follows [14] :

$$C_{SH} = \sqrt{\frac{C_{66}}{\rho_0}} \qquad (5)$$

where C_{66} is the corresponding elastic coefficient of the interfacial material and ρ_0 its density.

For the considered values of P in Figure 8, δ varies from 46 (for $P = 0.1$) to 34 (for $P = 0.9$). When P increases, the values of the shear moduli decrease (Figure 7). The decrease of these moduli is synonymous with the decrease of C_{SH} which implies the decrease of the associated wavelength. This, translates to the decrease of the δ ratio (with h kept constant). Finally, δ is dependent on P and the increase of P implies the reduction of δ.

Figure 8 indicates that when the porosity factor increases, the shift of the peaks with respect to the perfect interface case increases significantly. Indeed, the calculation of the correlation coefficient between the perfect case and the imperfect ones gives the results presented in Table 3.

Table 3: Evolution of the correlation coefficient with respect to the porosity factor.

Porosity factor	Correlation coefficient
$P = 0.1$	0.75
$P = 0.5$	0.22
$P = 0.9$	0.09

Thus, the study of the correlation coefficient and the peaks positions could be a way to characterize the adherence quality at the interface via experimental measurements.

In order to verify the coherence of the simulation results for anisotropic multilayers, Figure 9 presents a comparison of the reflectance functions obtained between Nickel (20 μm) on Zinc (20 μm) bilayers with different interfaces. One interface is perfect, the second is an interface layer of 100 nm thickness with a porosity factor equal to 0.01 and finally an interface layer of 500 nm thickness with the same porosity factor. Figure 9 illustrates the fact that for a very low porosity factor, the reduction of the thickness of the interface layer makes the value of the reflectance function tend towards the value obtained with a perfect interface. Indeed, the correlation coefficient between the perfect interface and the imperfect ones grows from 0.82 for $h = 500\,nm$ to 0.99 for $h = 100\,nm$. This can be explained by the fact that the wavelength of the waves inside the structure becomes much larger than the thickness of the interface layer. Hence, the influence of the interface layer tends to disappear.

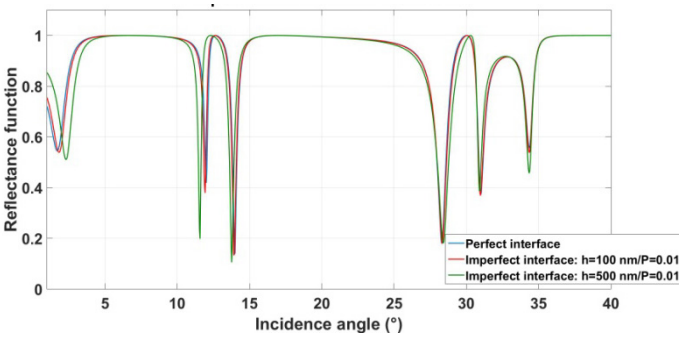

Figure 9: Comparison between the magnitude of the reflectance functions obtained for a multilayer with a perfect interface and multilayers containing imperfect interfaces with very low porosity and variable thicknesses.

4 Conclusion and future work

Models have been implemented to calculate reflectance functions for immersed multilayers. Two different models have been implemented to take into account isotropic and anisotropic materials. In each case, the quality of adhesion between successive layers was considered. Interfacial layers whose thicknesses are much smaller than the wavelengths involved represent the imperfect interfaces.

In the isotropic case, a virtual viscoelastic material models the interface layer and the quality of adhesion is affected by the viscoelasticity of the medium. For

anisotropic materials, an orthotropic porous material obtained using the Hill's approximation and the Christensen's composite model represents the interface layer. The quality of adhesion at the interface in the anisotropic case can be modified through the porosity factor and the orientation of the pores.

Depending on the frequency of the incident wave, the studied structure can be just seen as a multilayer or a multilayer deposited on a substrate. The calculations have to be changed accordingly and works are in progress in regard to this latter case.

In the results presented for the anisotropic imperfect interface layer, the pores were all directed along the x_1 axis. In the future, the influence of the pores deviation from the x_1 axis will be studied.

The reflectance functions obtained by modeling, will be included in algorithms allowing to compute the V(z) responses associated with them. Thus, it could be envisaged to characterize interface defects by experimental measurements based on the treatment of the V(z) responses.

Acknowledgement

This work has been supported by the co-labelled EURIPIDES² and CATRENE project SAM³ (Smart Analysis Methods for 3D Integration).

References

[1] J.D. Achenbach, Wave Propagation in Elastic Solids, North-Holland Publishing Company, 1973.

[2] L.M. Brekhovskikh, Waves in layered media, Academic Press, 1960.

[3] G.J. Kühn, A. Lutsch, Elastic Wave Mode Conversion at a Solid-Solid Boundary with Transverse Slip, J. Acoust. Soc. Am. 33 (1961) 949–954.

[4] W.T. Thomson, Transmission of Elastic Waves through a Stratified Solid Medium, J. Appl. Phys. 21 (1950) 89–93.

[5] N.A. Haskell, The dispersion of surface waves on multilayered media, Bull. Seismol. Soc. Am. 43 (1953) 17–34.

[6] M. Lematre, Contribution de la microscopie acoustique à la caractérisation des matériaux : Application à la détermination des constantes élastiques, Université de Valenciennes et du Hainaut Cambrésis, 2000.

[7] S.I. Rokhlin, W. Huang, Ultrasonic wave interaction with a thin anisotropic layer between two anisotropic solids: Exact and asymptotic-boundary-condition methods, J. Acoust. Soc. Am. 92 (1992) 1729–1742.

[8] S.I. Rokhlin, Y.J. Wang, Analysis of boundary conditions for elastic wave interaction with an interface between two solids, J. Acoust. Soc. Am. 89 (1991) 503–515.

[9] A.I. Lavrentyev, S.I. Rokhlin, Models for ultrasonic characterization of environmental degradation of interfaces in adhesive joints, J. Appl. Phys. 76 (1994) 4643–4650.

[10] R. Hill, The Elastic Behaviour of a Crystalline Aggregate, Proc. Phys. Soc. Sect. A. 65 (1952) 349.

[11] R.M. Christensen, Mechanics of Composite Materials, Krieger, Malabar, FL, 1991.

[12] A. Reuss, Berechnung der Fließgrenze von Mischkristallen auf Grund der Plastizitätsbedingung für Einkristalle ., ZAMM - J. Appl. Math. Mech. / Zeitschrift Für Angew. Math. Und Mech. 9 (1929) 49–58.

[13] W. Voigt, Lehrbuch der Kristallphysik, Leipzig, Teubner, 1928.

[14] S.I. Rokhlin, Y.J. Wang, Equivalent boundary conditions for thin orthotropic layer between two solids: Reflection, refraction, and interface waves, J. Acoust. Soc. Am. 91 (1992) 1875–1887.

[15] D. Tromans, Elastic Anisotropy of HCP Metal Crystals and Polycrystals, 2011.